

# Enhancing Adversarial Transferability via Component-Wise Augmentation Method

Hangyu Liu<sup>1,2\*</sup>, Bo Peng<sup>2</sup>, Pengxiang Ding<sup>1,3</sup>, Donglin Wang<sup>1†</sup>

<sup>1</sup>Westlake University, <sup>2</sup>Beijing University of Posts and Telecommunications, <sup>3</sup>Zhejiang University

## Abstract

Deep Neural Networks (DNNs) are highly vulnerable to adversarial examples, which pose significant challenges in security-sensitive applications. Among various adversarial attack strategies, input transformation-based attacks have demonstrated remarkable effectiveness in enhancing adversarial transferability. However, existing methods fail to diversify attention regions across models adequately and introduce excessive information loss during transformations. In this paper, we introduce a novel input transformation-based method, termed Component-Wise Augmentation (CWA), designed to enhance transferability by locally applying block-wise transformations. CWA strategically integrates interpolation and selective rotation on individual image blocks to diversify model attention regions while preserving semantic integrity. Extensive experiments on the standard ImageNet dataset show that CWA consistently outperforms state-of-the-art methods in both attack success rates and stability across CNN- and Transformer-based models, while also demonstrating superior performance against multiple defense methods.

## 1. Introduction

With the rapid development of deep learning, artificial intelligence has achieved significant progress in computer vision, finding widespread applications in tasks such as image classification [11, 13], object detection [30, 31], and semantic segmentation [23, 32]. However, the adversarial vulnerability of deep learning models has gradually surfaced as a critical issue, limiting their deployment in real-world scenarios. Research shows that carefully crafted adversarial examples—created by adding imperceptible perturbations to normal input data—can cause deep learning models to make erroneous predictions [9, 10, 37]. This phenomenon not only affects model performance on standard test datasets but poses severe risks in high-stakes applications [6, 36, 52]

\*This work was done while Hangyu Liu was an intern at Westlake Milab.

†Corresponding author.

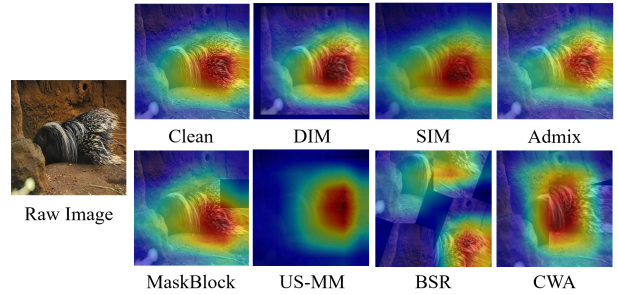


Figure 1. The heatmaps generated on ResNet-18 of raw image and its **transformed images** by DIM, SIM, Admix, MaskBlock, US-MM, BSR, and our proposed CWA.

such as autonomous driving and medical diagnostics.

In black-box scenarios, attackers lack access to the details of the target models and can only rely on a limited number of surrogate models to craft adversarial examples. Therefore, a critical challenge is transferability, which refers to the ability of adversarial examples generated on surrogate models to deceive other target models, even when the target models have different architectures or are trained on different datasets [40, 49].

To improve adversarial transferability, researchers have proposed a variety of methods for generating adversarial examples. Gradient-based methods [4, 8, 9, 16, 20] leverage the gradient information of models to craft adversarial examples with high computational efficiency and serve as the foundation for many other approaches. However, they generally suffer from poor transferability, particularly across models with different architectures. Model-related methods [24, 46, 47] exploit internal model features, such as skip connections or backpropagation, to generate architecture-specific adversarial examples. While these methods perform well for specific architectures, they often overfit and lack generalizability, making them less effective for diverse architectures. Ensemble-based [1, 17, 21, 51] and generation-based [33] methods aggregate the outputs of multiple models or use generative models like GANs to directly generate adversarial examples. While these approaches can improve transferability, they are constrained by high computational

costs, reliance on joint training of multiple models, and limited scalability. In contrast, input transformation-based methods [20, 49, 49, 53] enhance cross-model transferability through enriching adversarial example diversity with operations such as cropping, scaling, and rotation. These methods are computationally efficient and do not require access to model parameters, making them particularly suitable for black-box attack scenarios.

However, current input transformation-based methods still face critical challenges. As shown in Figure 1, some methods fail to effectively shift the model’s attention, while others redirect attention to irrelevant regions of the object, introducing significant information loss in the process.

To address these issues, we propose a novel method called Component-Wise Augmentation (CWA), which enhances the transferability of adversarial examples by encouraging models to focus on diverse regions of the object in the original image. Specifically, CWA applies block-wise transformations that interpolate and selectively rotate image patches while preserving essential semantic information. By introducing these localized transformations, our method generates adversarial examples with enriched attention distributions that generalize effectively across different model architectures.

Our contributions can be summarized as follows:

1. **A New Perspective:** We provide a fresh perspective on solving the untargeted transferability challenge. Instead of broadly enriching input images, our approach focuses on crafting transformed images that maximize the diversity of attention regions within the object area in original input images.
2. **Novel Input Transformation Framework:** We propose CWA, an innovative method combining interpolation and selective rotation to enhance adversarial transferability by preserving semantic integrity while diversifying attention distributions.
3. **State-of-the-Art Performance:** Our method achieves state-of-the-art results on the ImageNet dataset, demonstrating superior attack success rates and lower standard deviations compared to existing approaches.

## 2. Related Work

### 2.1. Input Transformation-based Attacks

Input transformation-based methods have been widely studied to enhance adversarial transferability, particularly in black-box settings. These methods diversify the input samples used for gradient computation, enabling adversarial examples to generalize across different model architectures. We classify these methods into four categories: scale-based methods, mixed image-based methods, block-based methods, and adaptive-based methods. Scale-based methods [20, 49] focus on resizing and transforming input images to introduce diversity in gradient computation. Mixed image-based

methods [39, 41, 53] enrich input diversity by incorporating features from other images or categories. However, whole-image transformations alone may not effectively alter the model’s attention. To address this, Block-based methods [7, 38] focus on partitioning input images into blocks and applying transformations to each block independently. Furthermore, to better utilize existing transformation methods, adaptive-based methods [43, 45, 54] introduce learnable transformation strategies to optimize adversarial transferability.

### 2.2. Adversarial Defense

Various defense approaches have been proposed to mitigate the threat of adversarial attacks, including adversarial training [25, 42], feature denoising [48], certified defenses [10, 29] and diffusion purification [44]. Among these, AT [35] is one of the most effective methods, where adversarial examples are incorporated during training to enhance model robustness. HGD [19] utilizes a denoising autoencoder guided by high-level representations to eliminate adversarial perturbations. Similarly, NRP [26], leverages a self-supervised adversarial training mechanism to purify input samples, demonstrating strong effectiveness against transfer-based attacks. Certified defense methods, such as RS [3], train robust classifiers by adding noise to the input and providing provable robustness within a certain radius. Furthermore, diffusion purification such as Diffure [27] employs diffusion models to process input samples and reduce adversarial perturbations, further enhancing model resilience against adversarial threats.

## 3. Methodology

In this section, we first introduce the prerequisite knowledge and our motivation. Then, we provide a detailed explanation of our CWA method. To highlight the differences between our approach and other methods, we also summarize the distinctions between our method and DIM [49], as well as BSR [38].

### 3.1. Preliminaries

Given a target model  $f$  with parameters  $\theta$  and a clean input  $x$  with the ground-truth label  $y$ , the objective of an untargeted attacker is to generate an adversarial example  $x^{adv}$  that is visually similar to  $x$ , such that  $\|x^{adv} - x\|_p \leq \epsilon$  and causes the model to misclassify the input, meaning  $f(x^{adv}; \theta) \neq y$ . Here,  $\epsilon$  denotes the perturbation budget, and  $\|\cdot\|_p$  is the  $\ell_p$ -norm that quantifies the allowed perturbation. In this paper, we focus on the  $\ell_\infty$ -norm (where  $p = \infty$ ), which restricts the maximum change to each individual pixel.

To generate such an adversarial example, the attacker generally maximizes the loss function  $J(x^{adv}, y; \theta)$  (e.g., cross-entropy loss) with respect to  $x^{adv}$ , subject to the constraint  $\|x^{adv} - x\|_p \leq \epsilon$ . This can be formalized as follows:

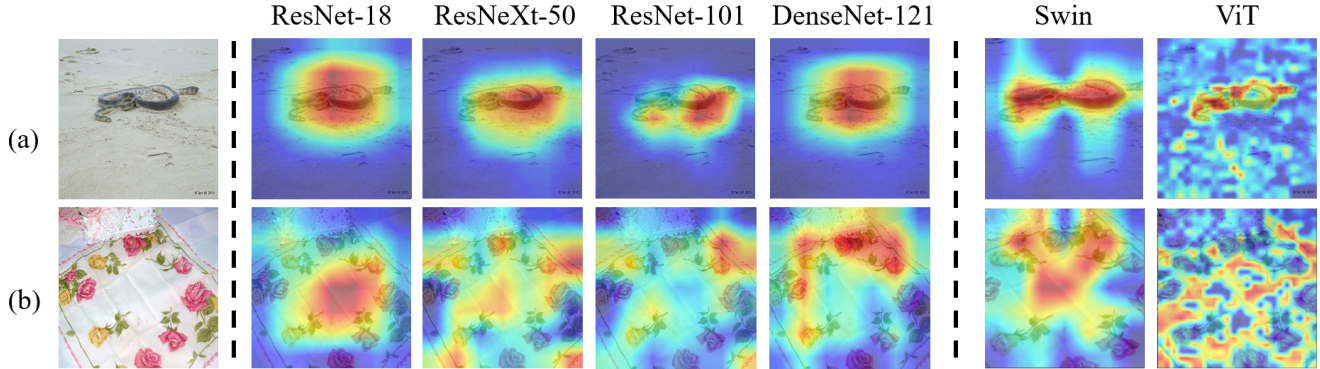


Figure 2. **Demonstration of the different discriminative regions of the different models.** We adopt Grad-CAM [34] to visualize the attention maps of four CNN-based models—ResNet-18, ResNext-50, ResNet-101, DenseNet-121 and two Transformer-base models—Swin, ViT.

$$x^{adv} = \arg \max_{\|x^{adv} - x\|_p \leq \epsilon} J(x^{adv}, y; \theta) \quad (1)$$

Many methods have been proposed to approximate this optimization. Among these, the Momentum Iterative Fast Gradient Sign Method (MI-FGSM) [4] is particularly notable for enhancing the transferability of adversarial examples across diverse models. This method incorporates a momentum term into the gradient calculation to stabilize the perturbation direction across iterations, thereby increasing the probability of successful attacks on various models. The update rule for the accumulated gradient  $g_t$  is:

$$g_{t+1} = \mu \cdot g_t + \frac{\nabla_x J(x_t^{adv}, y; \theta)}{\|\nabla_x J(x_t^{adv}, y; \theta)\|_1} \quad (2)$$

$$x_{t+1}^{adv} = x_t^{adv} + \alpha \cdot \text{sign}(g_{t+1}) \quad (3)$$

where  $\mu$  is the decay factor that controls the influence of previous gradients, and  $g_t$  is the accumulated gradient at iteration  $t$ . The  $\ell_1$ -normalization of the gradient helps maintain consistency in the perturbation direction across iterations, enhancing the transferability of the attack.

### 3.2. Motivation

Despite differences in architectures and parameters, models trained for the same task often exhibit similar decision boundaries due to a shared latent space [15]. Adversarial attacks leveraging input transformations aim to generate diverse perturbations, enabling gradient-based methods to effectively explore this shared latent space and identify vulnerabilities in model decision boundaries.

However, experiments reveal a critical limitation: adversarial examples that perform well on the surrogate model often fail to generalize effectively to target models. This observation raises an important question:

*Why does this discrepancy occur?*

As illustrated in Figure 2, we observe that even when classification results are identical, the attention distributions of different models vary significantly. For instance, as shown in Figure 2(a), ResNet-18 focuses on the belly of the snake, while Swin focuses on both the head and tail of the snake. Motivated by these findings, we hypothesize that the transferability of adversarial attacks improves when perturbations better cover the regions of interest across all models. This hypothesis aligns with the principle of leveraging gradients from multiple models to optimize interactive perturbations.

To investigate this hypothesis, we first evaluate the attention distributions of transformed images generated by various input-transformation-based attack methods, as shown in Figure 1. It reveals that methods such as DIM, SIM, Admix, Maskblock, and US-MM fail to significantly alter the attention distributions. While BSR enriches the attention regions, it often shifts the focus to irrelevant areas outside the objects of interest in the original image. These findings prompt a novel question:

*How can we generate transformed images that encourage models to focus on diverse regions of the objects within an image?*

### 3.3. Component-Wise Augmentation

Encouraging models to focus on diverse regions of the object within an image is a challenging task for several reasons: 1) First, **models tend to concentrate their attention on the most salient features** of an object. Deep learning models are optimized to identify the most discriminative parts that contribute significantly to classification, often neglecting other informative regions. 2) Second, **the attention distribution is highly dependent on model architecture and training data**. Different models may attend to different regions of the same object, making it difficult to design a unified approach



that effectively diversifies attention across various models.

To address these challenges, a straightforward method is to apply **random masking** to the image, forcing the model to utilize other regions for prediction. However, this approach leads to significant information loss, as substantial parts of the image are obscured, potentially impairing the attack algorithm performance.

Therefore, we define our objectives as:

- **Maximize the retention of original image information:** Ensure that essential features and semantics of the original image are preserved to maintain the model’s performance.
- **Maximize the diversity of model attention regions:** Generate multiple transformed images where the model’s attention covers as much as possible the region where the object is located in the original image.

Motivated by human perception [28], where people tend to focus on larger objects, previous work [18] has also shown that models tend to pay attention to larger regions within an image. This insight suggests that we could apply a **zoom-in operation** to the image to enlarge the object, potentially shifting the model’s attention. However, globally scaling up the image fails to effectively change the relative size differences between different parts of the object and can cause significant displacement of the object from its original position.

To overcome these limitations, we propose **CWA**, which applies a sequence of transformations to individual blocks of an image. These transformations include **interpolation** (for more details on interpolation, refer to Appendix 7), comprising **pre-interpolation** (interpolation-based shrinking) and **block-wise scaling** (interpolation-based enlargement), as well as **selective rotation**. Together, these operations enhance local feature diversity and improve the model’s robustness against adversarial perturbations.

Formally, the CWA process involves the following steps:

1. **Image Partitioning:** Divide the image  $x$  into a grid of  $n \times n$  non-overlapping blocks  $\{B_{i,j}\}$ , where  $i, j \in \{1, 2, \dots, n\}$ .
2. **Pre-Interpolation:** For each block  $B_{i,j}$ , apply **scaled down** to reduce redundancy and compress features. Specifically,  $B_{i,j}$  is scaled by a random factor  $s_{i,j}$ , where:

$$s_{i,j} \sim \text{Uniform}[s_{\min}, s_{\max}], \quad (4)$$

The scaled-down block  $B'_{i,j}$  is calculated as:

$$B'_{i,j} = \text{Interpolate}(B_{i,j}, \text{size} = (H'_{i,j}, W'_{i,j})), \quad (5)$$

where:

$$H'_{i,j} = \lfloor H_{i,j}/s_{i,j} \rfloor, \quad W'_{i,j} = \lfloor W_{i,j}/s_{i,j} \rfloor. \quad (6)$$

The effectiveness of the Pre-Interpolation step is demonstrated in Figure 4, which shows how it contributes to reducing redundancy and improving adversarial robustness.

3. **Block-wise Scaling:** After pre-interpolation, each block is scaled up using the same scaling factor  $s_{i,j}$ , focusing attention on specific features. The scaled-up block  $\hat{B}_{i,j}$  is computed as:

$$\hat{B}_{i,j} = \text{Interpolate}(B'_{i,j}, \text{size} = (H''_{i,j}, W''_{i,j})), \quad (7)$$

where:

$$H''_{i,j} = \lfloor H_{i,j} \cdot s_{i,j} \rfloor, \quad W''_{i,j} = \lfloor W_{i,j} \cdot s_{i,j} \rfloor. \quad (8)$$

4. **Selective Rotation:** To further diversify the spatial representation of features and avoid the massive information loss caused by rotating all blocks, Selective Rotation is applied to a subset of blocks. Let  $N$  be the total number of blocks, and let  $\mathcal{R} \subseteq \{1, 2, \dots, N\}$  denote the indices of  $k$  randomly selected blocks for rotation ( $|\mathcal{R}| = k$ ). For each selected block  $B_{i,j} \in \mathcal{R}$ , a random rotation angle  $r_{i,j}$  is sampled from:

$$r_{i,j} \sim \text{Uniform}(-r_{\max}, r_{\max}), \quad (9)$$

where  $r_{\max}$  defines the allowable rotation range. The block is rotated around its center, and any padding is filled with zeros to maintain the original dimensions.

5. **Random Cropping:** After scaling and optional rotation, each block  $\hat{B}_{i,j}$  is cropped back to its original size  $H_{i,j} \times W_{i,j}$ .
6. **Image Reconstruction:** After all transformations are applied to each block, the blocks are reassembled into a single transformed image:

$$T_k(I) = \bigcup_{i=1}^n \bigcup_{j=1}^n \tilde{B}_{i,j}. \quad (10)$$

To stabilize gradient calculations during adversarial training with CWA, we compute the average gradient over  $N$  transformed images:

$$\bar{g} = \frac{1}{N} \sum_{i=1}^N \nabla_{x^{\text{adv}}} J(T(x^{\text{adv}}, n, N, s_{\max}, k, r), y; \theta) \quad (11)$$

Where  $T(x, n, N, s_{\max}, k, r)$  represents the transformation applied to the augmented image, parameterized by the input image  $x$ , the number of blocks  $n$ , the total number of transformed images  $N$ , the maximum scaling factor  $s_{\max}$  (with  $s_{\min} = 1.0$ ), the maximum rotation angle  $r$ , and the number of rotated blocks  $k$ .  $J$  denotes the loss function (e.g., cross-entropy), and  $y$  is the ground truth label.

Here we integrate our CWA method into MI-FGSM, and summarize the algorithm in Algorithm 1

### 3.4. Comparison of CWA with DIM and BSR

DIM enhances the transferability of adversarial attacks by applying resizing and padding to input samples, whereas

---

**Algorithm 1** Component-Wise Augmentation

---

**Require:** A classifier  $f$  with parameters  $\theta$ , loss function  $J$ , a raw example  $x$  with ground-truth label  $y$ , the magnitude of perturbation  $\epsilon$ , learning rate  $\alpha$ , decay factor  $\mu$ , number of iterations  $T$ , number of transformed images  $N$ , number of blocks  $n$ , the maximum scaling factor  $s_{\max}$ , the maximum rotation angle  $r$ , and the number of rotated blocks  $k$ .

**Ensure:** An adversarial example  $x^{\text{adv}}$ .

- 1: Initialize  $\delta = 0$ ,  $g_0 = 0$ , and  $\alpha = \epsilon/T$
- 2: **for**  $t = 1 \rightarrow T$  **do**
- 3:   Calculate the gradient by Eq. 11.
- 4:   Update the momentum  $g_t$  by:

$$g_t = \mu \cdot g_{t-1} + \frac{\bar{g}}{\|\bar{g}\|_1}$$

- 5:   Update the adversarial perturbation  $\delta$  by:

$$\delta = \alpha \cdot \text{sign}(g_t)$$

- 6:   Clip  $\delta$  to ensure  $\|\delta\|_\infty \leq \epsilon$
- 7:   Update the adversarial example by:

$$x_t^{\text{adv}} = x_{t-1}^{\text{adv}} + \delta$$

8: **end for**

9: **return**  $x_T^{\text{adv}}$

---

BSR achieves this by randomly shuffling and rotating image blocks. Despite incorporating similar operations, our method, CWA, differs significantly from these approaches. Below, we highlight the distinctions between our method and the two techniques.

- **CWA Vs. DIM** In contrast to DIM, which performs scaling with fixed values on the entire image, our method emphasizes a random enlargement operation with pre-interpolation. Moreover, while DIM applies this operation to the entire image uniformly, our approach targets individual blocks within the image, introducing more localized transformations.
- **CWA Vs. BSR** As for BSR, although both methods involve block partitioning, our approach discards the shuffle operation and primarily utilizes block interpolation to modify the image structure. Regarding rotation, instead of applying rotation to all blocks, our method adopts a selective rotation mechanism, where the number of rotated blocks is limited.

## 4. Experiments

### 4.1. Experimental Setup

**Models.** We evaluate our proposed CWA method across three categories of target models: 1) **CNN-based models**, including four widely recognized architectures: ResNet-

18 [11], ResNet-101 [11], ResNeXt-50 [50], and DenseNet-121 [14]; 2) **Transformer-based models**, comprising ViT-B [5], PiT [12], Visformer [2], and Swin [22]; 3) **Defense models**, which include five defense methods: AT [35], HGD [19], neural NRP [26], RS [3], and DiffPure [27]; All models are pre-trained on the ImageNet dataset and evaluated on single model.

**Dataset.** Following previous works<sup>1</sup>, We evaluate our proposed CWA on 1000 images belonging to 1000 categories from the validation set of ImageNet dataset. All images are classified correctly by the models.

**Baselines.** We compare CWA with other input transformation-based methods. Specifically, the image scale-based methods (DIM [49], SIM [20]), the mixed image-based methods (Admix [41], US-MM [39]), and the block-based methods (MaskBlock [7], BSR [38]). For fairness, all the input transformations are integrated into MI-FGSM [4].

**Evaluation Settings.** We set the maximum perturbation  $\epsilon = 16/255$ , the number of iterations  $epoch = 10$ , the step size  $\alpha = \epsilon/epoch$ , the batch size  $batchsize = 8$ , and the decay factor  $\mu = 1$  for MI-FGSM. For our method, CWA generates 20 scaled copies per iteration, divides the image into 2x2 blocks, applies a scaling factor ranging from 1.0 to 1.3, and applies a maximum rotation angle of  $26^\circ$ , selectively rotating  $k = 2$  blocks. For other methods, we follow the parameters reported in the original papers. But for US-MM, we modify the number of scaled copies to 20 per iteration for fairness.

### 4.2. Evaluations on CNN-based Models

We first evaluate the transferability of adversarial examples generated by various attacks with input transformations when the surrogate model is based on a CNN architecture. Specifically, we generate adversarial examples using ResNet-18, ResNet-101, ResNeXt-50, and DenseNet-121 as surrogate models and evaluate their attack success rates (ASR) across eight target models. The results are summarized in Table 1, where the first column indicates the surrogate model, the second column lists the attack methods, and the remaining columns present the ASR of different classification models under attack and the last two columns are the mean ASR and standard deviation, respectively.

Our proposed method consistently achieves state-of-the-art performance, with the highest mean ASR and lowest standard deviation across almost all experimental settings. Notably, when the surrogate model is ResNet-18, our method achieves the highest ASR across all target models. Furthermore, when the target models are ViT and PiT, our method surpasses the previous state-of-the-art BSR more than 6.5% and outperforms other baseline methods by at least 24%.

These results confirm the effectiveness of our approach

---

<sup>1</sup><https://github.com/Trustworthy-AI-Group/TransferAttack>

Model	Attack	ResNet-18	ResNet-101	ResNeXt-50	DenseNet-121	ViT	PiT	Visformer	Swin	Mean	Std. Dev.
ResNet-18	DIM	<b>100*</b>	61.7	66.1	90.4	30.4	37.4	53.4	56.9	62.0	23.8
	SIM	<b>100*</b>	59.6	64.1	90.5	24.6	35.7	49.0	53.3	59.6	25.5
	Admix	<b>100*</b>	69.9	74.6	95.4	31.2	42.6	59.8	63.0	67.1	23.6
	MaskBlock	<b>100*</b>	48.8	50.4	79.6	18.6	25.3	38.4	43.7	50.6	27.1
	US-MM	<b>100.0*</b>	66.6	71.7	94.3	29.1	41.0	56.8	60.3	65.0	24.2
	BSR	<b>100.0*</b>	89.1	90.2	<b>99.4</b>	49.1	62.3	79.4	79.2	81.1	16.7
	CWA	<b>100.0*</b>	<b>90.2</b>	<b>93.7</b>	<b>99.4</b>	<b>55.9</b>	<b>68.8</b>	<b>84.1</b>	<b>83.6</b>	<b>84.5</b>	<b>14.3</b>
ResNet-101	DIM	61.7	84.7*	63.0	65.5	30.2	40.9	48.0	48.2	55.3	16.9
	SIM	62.5	91.7*	64.7	66.3	25.8	38.1	46.3	46.1	55.2	20.4
	Admix	74.7	94.9*	77.5	77.4	36.0	49.7	60.9	58.6	66.2	18.6
	MaskBlock	61.3	92.3*	56.6	61.9	19.5	29.8	36.5	38.5	49.6	23.2
	US-MM	81.8	<b>95.1*</b>	80.1	83.7	35.3	50.7	62.7	60.6	68.8	19.9
	BSR	86.7	94.6*	89.6	90.2	58.5	72.9	80.8	78.1	81.4	10.9
	CWA	<b>87.7</b>	<b>95.1*</b>	<b>91.0</b>	<b>91.6</b>	<b>67.3</b>	<b>78.5</b>	<b>85.5</b>	<b>81.9</b>	<b>84.8</b>	<b>8.3</b>
ResNeXt-50	DIM	61.3	55.8	86.7*	63.0	26.0	35.2	45.7	44.4	52.3	18.8
	SIM	59.5	57.8	94.0*	64.6	20.9	32.9	39.7	41.6	51.4	22.7
	Admix	71.8	72.9	95.8*	75.6	29.6	44.4	53.7	53.9	62.2	20.8
	MaskBlock	55.3	46.2	94.1*	54.5	16.4	24.2	32.5	33.1	44.5	24.4
	US-MM	78.6	73.2	<b>96.9*</b>	82.1	31.5	46.8	57.6	55.6	65.3	21.2
	BSR	85.7	86.0	96.5*	88.7	48.2	68.3	76.0	73.9	77.9	14.1
	CWA	<b>87.3</b>	<b>86.4</b>	95.9*	<b>90.2</b>	<b>57.7</b>	<b>72.3</b>	<b>80.9</b>	<b>78.4</b>	<b>81.1</b>	<b>11.2</b>
DenseNet-121	DIM	86.7	70.7	72.0	99.9*	34.0	43.6	60.6	57.2	65.6	21.6
	SIM	90.0	70.3	72.8	<b>100*</b>	31.5	41.0	57.0	59.6	65.3	23.1
	Admix	95.3	80.5	83.2	<b>100*</b>	39.0	51.6	68.7	68.7	73.4	20.8
	MaskBlock	82.8	59.3	61.9	<b>100*</b>	23.8	34.4	47.9	49.3	57.4	24.8
	US-MM	95.6	77.9	79.9	99.9*	38.1	48.8	67.6	65.3	71.6	21.3
	BSR	98.0	89.7	92.2	<b>100.0*</b>	52.1	66.9	81.6	79.4	82.5	15.3
	CWA	<b>99.0</b>	<b>90.9</b>	<b>93.8</b>	<b>100.0*</b>	<b>56.4</b>	<b>70.8</b>	<b>85.3</b>	<b>82.2</b>	<b>84.8</b>	<b>14.0</b>

Table 1. Attack success rates (%) on eight models under single model setting with various single input transformations. The surrogate models are **cnv-based**. \* indicates the surrogate model.

in generating transferable adversarial examples when the surrogate model is CNN-based.

### 4.3. Evaluations on Transformer-based models

Building on the results observed with CNN-based models, we next evaluate our method’s performance when the surrogate model is based on a transformer architecture. Specifically, we use transformer-based models, including ViT, PiT, Visformer, and Swin, as surrogate models to generate adversarial examples and evaluate their transferability. The results are summarized in Table 2.

From the results, we observe that our method also achieves SOTA performance in terms of both mean ASR and standard deviation across most of experimental settings when the surrogate model is transformer-based. Notably, when the surrogate model is ViT, our method does not achieve the highest ASR on the original classification model (ViT itself) but consistently achieves the best performance on all other classification models. This demonstrates the robustness and generalizability of our approach, as it effectively transfers adversarial examples to different target architectures, even when the surrogate model has inherent challenges in transferability.

### 4.4. Evaluations on Defense Method

To comprehensively assess the robustness of our proposed method against diverse defense mechanisms, we conducted

experiments under five defense settings: Adversarial Training (AT), High-level representation Guided Denoiser (HGD), Neural Representation Purifier (NRP), Randomized Smoothing (RS), and Diffusion Purification (Diffure), with the results for NRP included in the appendix 6. As summarized in Tables 3 through 6, our method, particularly CWA, consistently achieves the highest attack success rates across most of defense settings, outperforming BSR and other baseline methods. For instance, under Diffure, it outperforms BSR by 6.9% in mean ASR and exceeding weaker baselines by more than 20%. Even under RS, a certified defense known for its robustness, our method maintains competitive ASRs (e.g., 28.7% for ResNet-101 and 29.5% for Visformer), showcasing its resilience. These results validate the robustness and effectiveness of our approach across diverse defenses.

### 4.5. Ablation Study

To further evaluate the performance improvements introduced by CWA, we conduct ablation studies on five key hyperparameters and one critical step: *number of blocks  $n$* , *maximum scale factor  $s_{max}$* , *maximum rotation angle  $r$* , *number of rotated blocks  $k$* , *number of transformed copies  $N$* , and the key step *pre-interpolation*. All experiments are conducted using ResNet-101 as the surrogate model.

**On the number of blocks  $n$ .** The impact of block partitioning is illustrated in Figure 3 (a). When  $n = 1$ , CWA

Model	Attack	ResNet-18	ResNet-101	ResNeXt-50	DenseNet-121	ViT	PiT	Visformer	Swin	Mean	Std. Dev.
ViT	DIM	56.9	47.8	49.6	59.7	89.5*	54.0	55.0	61.7	59.3	13.1
	SIM	62.4	48.6	52.4	64.3	<b>99.1*</b>	57.8	58.7	71.9	64.4	15.7
	Admix	65.6	52.4	55.3	65.9	98.9*	61.3	63.5	73.1	67.0	14.4
	MaskBlock	59.3	41.4	44.1	59.1	98.9*	46.9	51.3	62.6	58.0	18.3
	US-MM	69.2	54.7	57.6	68.7	97.4*	61.8	65.0	75.9	68.8	13.4
	BSR	78.2	74.7	75.9	81.0	90.2*	81.5	79.2	81.6	80.3	<b>4.4</b>
	CWA	<b>78.3</b>	<b>75.3</b>	<b>77.2</b>	<b>81.6</b>	<b>93.1*</b>	<b>83.5</b>	<b>82.4</b>	<b>83.9</b>	<b>81.9</b>	5.1
PiT	DIM	59.5	50.5	54.5	62.2	47.9	91.6*	63.5	65.3	61.9	13.5
	SIM	58.6	45.4	48.7	60.1	38.3	97.7*	56.8	60.9	58.3	17.8
	Admix	60.4	47.7	51.8	60.4	42.9	94.6*	61.1	63.5	60.3	15.7
	MaskBlock	59.2	40.4	45.2	57.3	35.4	<b>99.2*</b>	55.9	57.2	56.2	19.5
	US-MM	66.1	54.1	56.4	64.8	45.0	93.9*	64.0	68.0	64.0	14.3
	BSR	82.9	80.8	84.0	86.5	75.0	97.8*	90.2	90.4	86.0	6.5
	CWA	<b>85.8</b>	<b>85.1</b>	<b>87.3</b>	<b>90.7</b>	<b>85.3</b>	97.8*	<b>92.6</b>	<b>92.6</b>	<b>90.0</b>	<b>4.3</b>
Visformer	DIM	71.2	63.7	67.1	75.2	53.4	71.0	95.1*	76.9	71.7	12.0
	SIM	68.1	60.5	62.4	72.0	49.7	65.9	96.7*	74.8	68.8	13.7
	Admix	75.1	67.0	70.6	78.3	56.5	72.8	97.0*	81.6	74.9	11.8
	MaskBlock	64.2	47.3	51.3	64.4	35.7	54.9	99.2*	65.2	60.3	18.7
	US-MM	82.1	70.5	73.6	83.3	56.2	73.7	97.6*	82.9	77.5	12.1
	BSR	<b>90.7</b>	86.9	<b>90.7</b>	93.5	73.3	88.9	<b>99.3*</b>	92.7	89.5	7.0
	CWA	89.1	<b>87.6</b>	89.9	<b>94.0</b>	<b>80.4</b>	<b>91.9</b>	99.1*	<b>93.7</b>	<b>90.7</b>	<b>5.1</b>
Swin	DIM	67.2	53.4	56.8	68.8	48.7	65.3	69.3	96.2*	65.7	14.5
	SIM	48.9	29.9	34.1	45.4	27.7	35.5	43.1	98.1*	45.3	22.6
	Admix	55.1	33.9	37.4	50.0	28.3	37.8	47.2	98.2*	48.5	22.0
	MaskBlock	47.8	26.5	30.9	44.5	24.4	31.6	39.1	98.3*	42.9	23.9
	US-MM	57.5	32.2	37.8	52.2	26.8	37.8	47.4	96.8*	48.6	22.0
	BSR	88.7	82.5	86.0	91.2	71.6	89.7	91.0	98.3*	87.4	7.3
	CWA	<b>90.7</b>	<b>85.9</b>	<b>88.1</b>	<b>93.6</b>	<b>80.8</b>	<b>92.9</b>	<b>94.1</b>	<b>98.5*</b>	<b>90.6</b>	<b>5.2</b>

Table 2. Attack success rates (%) on eight models under single model setting with various single input transformations. The surrogate models are **transformer-based**. \* indicates the surrogate model.

Attack	ResNet-18	ResNet-101	ResNeXt-50	DenseNet-121	ViT	PiT	Visformer	Swin
DIM	36.4	32.9	32.0	34.6	33.4	33.2	33.5	33.7
SIM	36.5	31.6	32.1	35.6	35.4	33.4	34.3	31.0
ADMIX	38.4	32.6	32.2	38.0	35.9	33.5	34.3	31.8
MaskBlock	34.0	31.7	31.3	32.6	33.7	32.6	32.2	31.0
US-MM	38.3	34.9	33.7	37.9	36.4	34.8	35.4	32.0
BSR	40.3	36.9	35.2	38.9	<b>38.0</b>	35.1	36.7	37.5
CWA	<b>41.1</b>	<b>38.0</b>	<b>36.9</b>	<b>39.9</b>	37.7	<b>36.9</b>	<b>37.7</b>	<b>39.4</b>

Table 3. Attack success rates (%) of adversarial examples generated using various attack methods across eight classification models under **AT**.

Attack	ResNet-18	ResNet-101	ResNeXt-50	DenseNet-121	ViT	PiT	Visformer	Swin
DIM	24.4	29.8	20.7	27.2	25.7	23.4	26.8	21.1
SIM	23.3	28.9	18.0	24.7	27.8	20.9	25.9	14.2
ADMIX	24.2	35.2	23.3	30.5	28.9	23.1	29.3	14.9
MaskBlock	18.8	22.7	15.5	20.2	23.5	21.8	21.1	12.9
US-MM	24.5	33.8	23.2	27.0	30.1	23.3	29.4	13.8
BSR	33.6	45.5	28.8	33.8	39.5	35.0	37.9	30.5
CWA	<b>40.5</b>	<b>56.7</b>	<b>38.4</b>	<b>41.3</b>	<b>43.2</b>	<b>43.2</b>	<b>48.7</b>	<b>37.8</b>

Table 4. Attack success rates (%) of adversarial examples generated using various attack methods across eight classification models under **Diffuse**. The classifier is ResNet-101.

applies global operations to the entire image, which fails to sufficiently disrupt the attention heatmaps. Increasing  $n$  to 2 significantly improves the attack success rate, as the  $2 \times 2$  block division introduces localized transformations, encouraging the model to focus on diverse regions of the object. When  $n > 2$ , performance begins to degrade due to increased information loss from operating on a larger number of blocks. However, in contrast to BSR, the per-

Attack	ResNet-18	ResNet-101	ResNeXt-50	DenseNet-121	ViT	PiT	Visformer	Swin
DIM	56.9	49.7	42.1	66.7	43.0	45.7	57.2	46.2
SIM	52.7	43.5	36.4	64.3	42.4	37.2	49.1	22.5
ADMIX	63.1	58.2	50.6	76.5	46.8	39.9	57.2	25.9
MaskBlock	38.2	34.0	26.8	48.9	35.9	32.3	36.9	20.5
US-MM	59.4	60.1	52.2	72.5	48.2	44.8	61.2	24.5
BSR	86.9	80.9	74.9	90.1	71.9	74.2	81.0	75.0
CWA	<b>91.2</b>	<b>85.4</b>	<b>81.9</b>	<b>93.1</b>	<b>73.9</b>	<b>81.8</b>	<b>85.0</b>	<b>83.5</b>

Table 5. Attack success rates (%) of adversarial examples generated using various attack methods across eight classification models under **HGD**.

Attack	ResNet-18	ResNet-101	ResNeXt-50	DenseNet-121	ViT	PiT	Visformer	Swin
DIM	26.0	21.9	22.0	25.2	23.6	22.2	22.9	22.9
SIM	26.0	21.3	21.3	26.0	25.2	22.7	24.0	21.5
ADMIX	27.9	22.7	22.5	27.8	26.0	22.6	24.2	21.1
MaskBlock	23.8	21.2	20.8	23.0	23.6	22.4	22.1	20.5
US-MM	27.6	23.8	23.7	26.4	26.8	24.1	25.8	21.8
BSR	27.8	26.2	25.1	26.7	27.3	26.0	26.1	24.9
CWA	<b>30.9</b>	<b>28.7</b>	<b>27.9</b>	<b>30.8</b>	<b>29.3</b>	<b>27.8</b>	<b>29.5</b>	<b>28.7</b>

Table 6. Attack success rates (%) of adversarial examples generated using various attack methods across eight classification models under **RS**. The defense model used is ResNet-50 with a noise level of 0.50.

formance does not drop sharply, as our selective rotation method stabilizes the results. Consequently, we set  $n = 2$ .

**On the maximum scale factor  $s_{\max}$ .** As shown in Figure 3 (b), the maximum scale factor significantly impacts the ASR. When  $s_{\max} > 1.4$ , the ASR starts to decline gradually. This decline is due to the larger resizing requiring a random crop-

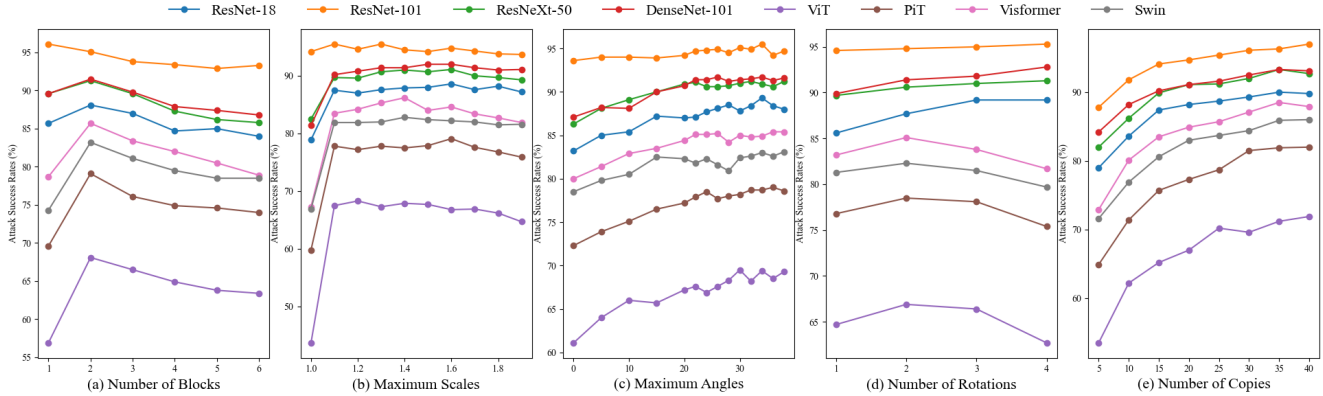


Figure 3. Attack success rates (%) of various models on the adversarial examples generated by CWA with different numbers of blocks, maximum resize rates, maximum rotate angles, numbers of rotation blocks and numbers of transformed copies. The adversarial examples are crafted using the ResNet-101 model and tested on seven other models under the black-box setting.

ping operation, and as the image is enlarged, the cropped areas become larger, leading to information loss. Therefore, we set  $s_{\max} = 1.3$  as the optimal value for our experiments.

**On the maximum rotation angle  $r$ .** As demonstrated in Figure 3 (c), we observe that gradually increasing  $r$  improves ASR, but fluctuations occur when the angle exceeds  $25^\circ$ . Considering the experimental error margins, we interpret this fluctuation as insignificant, and thus we select  $r = 26^\circ$  as the optimal value.

**On the number of rotated blocks  $k$ .** As shown in Figure 3 (d), we find that increasing  $k$  generally leads to a decline in performance on most target models. This is due to the additional padding introduced by more rotation operations, which results in increased information loss. Therefore, we select  $k = 2$  as the optimal value.

**On the number of transformed copies  $N$ .** As shown in Figure 3 (e), the ASR steadily improves with increasing  $N$ , as it stabilizes gradient updates and introduces greater diversity. However, to maintain consistency with the BSR baseline and minimize computational overhead, we set  $N = 20$  in our experiments.

**On pre-interpolation.** As shown in Figure 4, we observe that pre-interpolation significantly improves the performance of the method. This demonstrates its ability to effectively remove redundant information, thereby enabling the model to focus on the relevant regions of the transformed image.

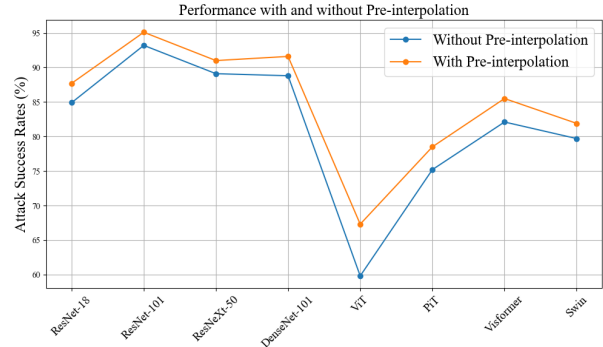


Figure 4. Attack success rates (%) of various models on the adversarial examples generated by CWA with and without Pre-interpolation. The surrogate model is ResNet-101.

## 5. Conclusion

Based on the observation that inconsistent attention distributions across models are a major barrier to adversarial example transferability, we propose CWA, a method utilizing interpolation and selective rotation. CWA effectively generates diverse transformed images, enriching the attention distributions of individual models and reducing discrepancies in gradient loss calculations across different models. Experimental results demonstrate that our approach not only surpasses existing SOTA methods in ASR but also achieves significantly lower standard deviation, highlighting its stability and generalization capabilities. Furthermore, CWA offers a fresh perspective for input transformation-based adversarial attacks.



## References

- [1] Bin Chen, Jiali Yin, Shukai Chen, Bohao Chen, and Ximeng Liu. An adaptive model ensemble adversarial attack for boosting adversarial transferability. In *Proceedings of the IEEE/CVF International Conference on Computer Vision*, pages 4489–4498, 2023. 1
- [2] Zhengsu Chen, Lingxi Xie, Jianwei Niu, Xuefeng Liu, Longhui Wei, and Qi Tian. Visformer: The vision-friendly transformer. In *Proceedings of the IEEE/CVF international conference on computer vision*, pages 589–598, 2021. 5
- [3] Jeremy Cohen, Elan Rosenfeld, and Zico Kolter. Certified adversarial robustness via randomized smoothing. In *international conference on machine learning*, pages 1310–1320. PMLR, 2019. 2, 5
- [4] Yinpeng Dong, Fangzhou Liao, Tianyu Pang, Hang Su, Jun Zhu, Xiaolin Hu, and Jianguo Li. Boosting adversarial attacks with momentum. In *Proceedings of the IEEE conference on computer vision and pattern recognition*, pages 9185–9193, 2018. 1, 3, 5
- [5] Alexey Dosovitskiy. An image is worth 16x16 words: Transformers for image recognition at scale. *arXiv preprint arXiv:2010.11929*, 2020. 5
- [6] Kevin Eykholt, Ivan Evtimov, Earlene Fernandes, Bo Li, Amir Rahmati, Chaowei Xiao, Atul Prakash, Tadayoshi Kohno, and Dawn Song. Robust physical-world attacks on deep learning visual classification. In *Proceedings of the IEEE conference on computer vision and pattern recognition*, pages 1625–1634, 2018. 1
- [7] Mingyuan Fan, Cen Chen, Ximeng Liu, and Wenzhong Guo. Maskblock: Transferable adversarial examples with bayes approach. *arXiv preprint arXiv:2208.06538*, 2022. 2, 5
- [8] Lianli Gao, Qilong Zhang, Jingkuan Song, Xianglong Liu, and Heng Tao Shen. Patch-wise attack for fooling deep neural network. In *Computer Vision—ECCV 2020: 16th European Conference, Glasgow, UK, August 23–28, 2020, Proceedings, Part XXVIII 16*, pages 307–322. Springer, 2020. 1
- [9] Ian J Goodfellow, Jonathon Shlens, and Christian Szegedy. Explaining and harnessing adversarial examples. *arXiv preprint arXiv:1412.6572*, 2014. 1
- [10] Sven Gowal, Krishnamurthy Dj Dvijotham, Robert Stanforth, Rudy Bunel, Chongli Qin, Jonathan Uesato, Relja Arandjelovic, Timothy Mann, and Pushmeet Kohli. Scalable verified training for provably robust image classification. In *Proceedings of the IEEE/CVF International Conference on Computer Vision*, pages 4842–4851, 2019. 1, 2
- [11] Kaiming He, Xiangyu Zhang, Shaoqing Ren, and Jian Sun. Deep residual learning for image recognition. In *Proceedings of the IEEE conference on computer vision and pattern recognition*, pages 770–778, 2016. 1, 5
- [12] Byeongho Heo, Sangdoon Yun, Dongyoon Han, Sanghyuk Chun, Junsuk Choe, and Seong Joon Oh. Rethinking spatial dimensions of vision transformers. In *Proceedings of the IEEE/CVF international conference on computer vision*, pages 11936–11945, 2021. 5
- [13] Jie Hu, Li Shen, and Gang Sun. Squeeze-and-excitation networks. In *Proceedings of the IEEE conference on computer vision and pattern recognition*, pages 7132–7141, 2018. 1
- [14] Gao Huang, Zhuang Liu, Laurens Van Der Maaten, and Kilian Q Weinberger. Densely connected convolutional networks. In *Proceedings of the IEEE conference on computer vision and pattern recognition*, pages 4700–4708, 2017. 5
- [15] Minyoung Huh, Brian Cheung, Tongzhou Wang, and Phillip Isola. The platonic representation hypothesis. *arXiv preprint arXiv:2405.07987*, 2024. 3
- [16] Alexey Kurakin, Ian J Goodfellow, and Samy Bengio. Adversarial examples in the physical world. In *Artificial intelligence safety and security*, pages 99–112. Chapman and Hall/CRC, 2018. 1
- [17] Qizhang Li, Yiwen Guo, Wangmeng Zuo, and Hao Chen. Making substitute models more bayesian can enhance transferability of adversarial examples. *arXiv preprint arXiv:2302.05086*, 2023. 1
- [18] Yanghao Li, Yuntao Chen, Naiyan Wang, and Zhaoxiang Zhang. Scale-aware trident networks for object detection. In *Proceedings of the IEEE/CVF international conference on computer vision*, pages 6054–6063, 2019. 4
- [19] Fangzhou Liao, Ming Liang, Yinpeng Dong, Tianyu Pang, Xiaolin Hu, and Jun Zhu. Defense against adversarial attacks using high-level representation guided denoiser. In *Proceedings of the IEEE conference on computer vision and pattern recognition*, pages 1778–1787, 2018. 2, 5
- [20] Jiadong Lin, Chuanbiao Song, Kun He, Liwei Wang, and John E Hopcroft. Nesterov accelerated gradient and scale invariance for adversarial attacks. *arXiv preprint arXiv:1908.06281*, 2019. 1, 2, 5
- [21] Yanpei Liu, Xinyun Chen, Chang Liu, and Dawn Song. Delving into transferable adversarial examples and black-box attacks. *arXiv preprint arXiv:1611.02770*, 2016. 1
- [22] Ze Liu, Yutong Lin, Yue Cao, Han Hu, Yixuan Wei, Zheng Zhang, Stephen Lin, and Baining Guo. Swin transformer: Hierarchical vision transformer using shifted windows. In *Proceedings of the IEEE/CVF international conference on computer vision*, pages 10012–10022, 2021. 5
- [23] Jonathan Long, Evan Shelhamer, and Trevor Darrell. Fully convolutional networks for semantic segmentation. In *Proceedings of the IEEE conference on computer vision and pattern recognition*, pages 3431–3440, 2015. 1
- [24] Avery Ma, Amir-massoud Farahmand, Yangchen Pan, Philip Torr, and Jindong Gu. Improving adversarial transferability via model alignment. In *European Conference on Computer Vision*, pages 74–92. Springer, 2025. 1
- [25] Aleksander Madry. Towards deep learning models resistant to adversarial attacks. *arXiv preprint arXiv:1706.06083*, 2017. 2
- [26] Muzammal Naseer, Salman Khan, Munawar Hayat, Fahad Shahbaz Khan, and Fatih Porikli. A self-supervised approach for adversarial robustness. In *Proceedings of the IEEE/CVF Conference on Computer Vision and Pattern Recognition*, pages 262–271, 2020. 2, 5
- [27] Weili Nie, Brandon Guo, Yujia Huang, Chaowei Xiao, Arash Vahdat, and Anima Anandkumar. Diffusion models for adversarial purification. *arXiv preprint arXiv:2205.07460*, 2022. 2, 5
- [28] Michael J Proulx. Size matters: large objects capture attention in visual search. *PLoS one*, 5(12):e15293, 2010. 4

- [29] Aditi Raghunathan, Jacob Steinhardt, and Percy Liang. Certified defenses against adversarial examples. *arXiv preprint arXiv:1801.09344*, 2018. 2
- [30] Joseph Redmon. Yolov3: An incremental improvement. *arXiv preprint arXiv:1804.02767*, 2018. 1
- [31] Shaoqing Ren, Kaiming He, Ross Girshick, and Jian Sun. Faster r-cnn: Towards real-time object detection with region proposal networks. *IEEE transactions on pattern analysis and machine intelligence*, 39(6):1137–1149, 2016. 1
- [32] Olaf Ronneberger, Philipp Fischer, and Thomas Brox. U-net: Convolutional networks for biomedical image segmentation. In *Medical image computing and computer-assisted intervention–MICCAI 2015: 18th international conference, Munich, Germany, October 5-9, 2015, proceedings, part III 18*, pages 234–241. Springer, 2015. 1
- [33] Mathieu Salzmann et al. Learning transferable adversarial perturbations. *Advances in Neural Information Processing Systems*, 34:13950–13962, 2021. 1
- [34] Ramprasaath R Selvaraju, Abhishek Das, Ramakrishna Vedantam, Michael Cogswell, Devi Parikh, and Dhruv Batra. Grad-cam: Why did you say that? *arXiv preprint arXiv:1611.07450*, 2016. 3
- [35] Ali Shafahi, Mahyar Najibi, Mohammad Amin Ghiasi, Zheng Xu, John Dickerson, Christoph Studer, Larry S Davis, Gavin Taylor, and Tom Goldstein. Adversarial training for free! *Advances in neural information processing systems*, 32, 2019. 2, 5
- [36] Mahmood Sharif, Sruti Bhagavatula, Lujo Bauer, and Michael K Reiter. Accessorize to a crime: Real and stealthy attacks on state-of-the-art face recognition. In *Proceedings of the 2016 acm sigsac conference on computer and communications security*, pages 1528–1540, 2016. 1
- [37] C Szegedy. Intriguing properties of neural networks. *arXiv preprint arXiv:1312.6199*, 2013. 1
- [38] Kunyu Wang, Xuanran He, Wenxuan Wang, and Xiaosen Wang. Boosting adversarial transferability by block shuffle and rotation. In *Proceedings of the IEEE/CVF Conference on Computer Vision and Pattern Recognition*, pages 24336–24346, 2024. 2, 5
- [39] Tao Wang, Zijian Ying, Qianmu Li, et al. Boost adversarial transferability by uniform scale and mix mask method. *arXiv preprint arXiv:2311.12051*, 2023. 2, 5
- [40] Xiaosen Wang and Kun He. Enhancing the transferability of adversarial attacks through variance tuning. In *Proceedings of the IEEE/CVF conference on computer vision and pattern recognition*, pages 1924–1933, 2021. 1
- [41] Xiaosen Wang, Xuanran He, Jingdong Wang, and Kun He. Admix: Enhancing the transferability of adversarial attacks. In *Proceedings of the IEEE/CVF International Conference on Computer Vision*, pages 16158–16167, 2021. 2, 5
- [42] Xiaosen Wang, Chuanbiao Song, Liwei Wang, and Kun He. Multi-stage optimization based adversarial training. *arXiv preprint arXiv:2106.15357*, 2021. 2
- [43] Xiaosen Wang, Zeliang Zhang, and Jianping Zhang. Structure invariant transformation for better adversarial transferability. In *Proceedings of the IEEE/CVF International Conference on Computer Vision*, pages 4607–4619, 2023. 2
- [44] Zekai Wang, Tianyu Pang, Chao Du, Min Lin, Weiwei Liu, and Shuicheng Yan. Better diffusion models further improve adversarial training. In *International Conference on Machine Learning*, pages 36246–36263. PMLR, 2023. 2
- [45] Xingxing Wei and Shiji Zhao. Boosting adversarial transferability with learnable patch-wise masks. *IEEE Transactions on Multimedia*, 2023. 2
- [46] Zhipeng Wei, Jingjing Chen, Micah Goldblum, Zuxuan Wu, Tom Goldstein, and Yu-Gang Jiang. Towards transferable adversarial attacks on vision transformers. In *Proceedings of the AAAI Conference on Artificial Intelligence*, pages 2668–2676, 2022. 1
- [47] Dongxian Wu, Yisen Wang, Shu-Tao Xia, James Bailey, and Xingjun Ma. Skip connections matter: On the transferability of adversarial examples generated with resnets. *arXiv preprint arXiv:2002.05990*, 2020. 1
- [48] Cihang Xie, Yuxin Wu, Laurens van der Maaten, Alan L Yuille, and Kaiming He. Feature denoising for improving adversarial robustness. In *Proceedings of the IEEE/CVF conference on computer vision and pattern recognition*, pages 501–509, 2019. 2
- [49] Cihang Xie, Zhishuai Zhang, Yuyin Zhou, Song Bai, Jianyu Wang, Zhou Ren, and Alan L Yuille. Improving transferability of adversarial examples with input diversity. In *Proceedings of the IEEE/CVF conference on computer vision and pattern recognition*, pages 2730–2739, 2019. 1, 2, 5
- [50] Saining Xie, Ross Girshick, Piotr Dollár, Zhuowen Tu, and Kaiming He. Aggregated residual transformations for deep neural networks. In *Proceedings of the IEEE conference on computer vision and pattern recognition*, pages 1492–1500, 2017. 5
- [51] Yifeng Xiong, Jiadong Lin, Min Zhang, John E Hopcroft, and Kun He. Stochastic variance reduced ensemble adversarial attack for boosting the adversarial transferability. In *Proceedings of the IEEE/CVF conference on computer vision and pattern recognition*, pages 14983–14992, 2022. 1
- [52] Shengming Yuan, Qilong Zhang, Lianli Gao, Yaya Cheng, and Jingkuan Song. Natural color fool: Towards boosting black-box unrestricted attacks. *Advances in Neural Information Processing Systems*, 35:7546–7560, 2022. 1
- [53] Jianping Zhang, Jen-tse Huang, Wenxuan Wang, Yichen Li, Weibin Wu, Xiaosen Wang, Yuxin Su, and Michael R Lyu. Improving the transferability of adversarial samples by path-augmented method. In *Proceedings of the IEEE/CVF Conference on Computer Vision and Pattern Recognition*, pages 8173–8182, 2023. 2
- [54] Rongyi Zhu, Zeliang Zhang, Susan Liang, Zhuo Liu, and Chenliang Xu. Learning to transform dynamically for better adversarial transferability. In *Proceedings of the IEEE/CVF Conference on Computer Vision and Pattern Recognition*, pages 24273–24283, 2024. 2

# Enhancing Adversarial Transferability via Component-Wise Augmentation Method

## Supplementary Material

### 6. Extended Evaluations on Defense Methods

In this section, we present the performance of our method on NRP, as shown in Tables 7 and 8. Specifically, we apply NRP to process adversarial images generated by different defense methods, and subsequently evaluate their Attack Success Rate (ASR) using eight models. The results demonstrate that our method, CWA, achieves superior performance in terms of both ASR and standard deviation (std) when applied to CNN-based and transformer-based surrogate models. Notably, while maintaining a reduction in standard deviation, our approach consistently improves the ASR by an average of 5% over the previous state-of-the-art methods.

### 7. More Analysis on Interpolation

To better understand the role of interpolation in affecting model attention distributions, we conducted experiments using various interpolation methods (e.g., bilinear, bicubic, nearest neighbor, and area interpolation) under different scaling factors. As shown in Figure 5, scaling factors below 1.0 tend to disperse attention across irrelevant regions, reducing focus on critical object areas. Conversely, scaling factors significantly above 1.0 excessively concentrate attention on limited regions. Moderate scaling factors, typically ranging from 1.0 to 1.8, yield the most balanced attention distributions, effectively redistributing focus across diverse object regions. For example, as depicted in Figure 5(a), a scaling factor of 1.0 primarily directs attention to a person’s back, while a factor of 1.4 shifts focus towards the hips, and 1.8 further moves attention to the left shoulder.

In our method, we strategically apply a two-step process to achieve balanced attention redistribution. First, we perform a shrinking operation on each block to disperse attention and eliminate redundant information. Next, we enlarge the block, refocusing the previously dispersed attention on critical regions of the object. This two-step process effectively balances attention distribution and enhances the model’s robustness.

Moreover, the choice of interpolation method plays a critical role in shaping attention distributions. **Bicubic interpolation**, while smooth, often over-smooths attention maps, making it less effective at capturing distinct object regions. **Nearest neighbor interpolation** demonstrates insensitivity to scaling factors above 1.0. **Area interpolation**, on the other hand, is overly sensitive to scaling factors below 1.0, resulting in attention maps that collapse onto irrelevant regions and fail to preserve essential object features. In

contrast, **bilinear interpolation** achieves a balance between smoothness and precision, producing the most consistent and well-distributed attention maps.

Thus, we adopt bilinear interpolation in our method to ensure optimal attention distribution and robust adversarial performance.

Model	Attack	ResNet-18	ResNet-101	ResNeXt-50	DenseNet-121	ViT	PiT	Visformer	Swin	Mean	Std. Dev.
ResNet-18	DIM	98.9*	39.5	40.7	64.5	19.5	25.8	30.4	34.7	44.3	25.8
	SIM	99.5*	40.6	44.7	67.5	17.2	24.9	31.9	37.3	45.5	26.5
	Admix	<b>99.9*</b>	47.8	51.9	77.7	19.9	28.4	35.8	41.5	50.4	26.5
	MaskBlock	98.0*	32	35.5	57.5	13.6	19	25	28.1	38.6	27.4
	US-MM	99.4*	46.6	51.3	76.2	21.5	29.3	39.5	42.6	50.8	25.5
	BSR	98.8*	53.4	60.0	81.8	25.9	37.7	46.7	50.0	56.8	23.5
	CWA	99.4*	<b>58.6</b>	<b>64.9</b>	<b>87.4</b>	<b>33.5</b>	<b>43.7</b>	<b>52.4</b>	<b>55.2</b>	<b>61.9</b>	<b>21.9</b>
ResNet-101	DIM	54.4	56.8*	38.7	49.5	19.1	25	28.5	29.4	37.7	14.4
	SIM	55.7	62.6*	40.8	51	17.1	25.7	28.3	30.6	39.0	16.1
	Admix	60.9	75.7*	52.9	58.9	22.6	33.2	37.9	39.8	47.7	17.4
	MaskBlock	53.3	54.6*	35.6	47.3	13	19.2	23	24.9	33.9	16.2
	US-MM	99.4*	46.6	51.3	76.2	21.5	29.3	39.5	42.6	50.8	25.5
	BSR	71.9	73.4*	63.6	70.8	32.2	45.0	51.8	50.1	57.7	14.9
	CWA	<b>74.7</b>	<b>80.9*</b>	<b>68.9</b>	<b>75.3</b>	<b>40.4</b>	<b>52.4</b>	<b>58.2</b>	<b>57.3</b>	<b>63.5</b>	<b>13.7</b>
ResNeXt-50	DIM	54	32.8	57.4*	46.8	16	23	26.8	27.2	35.5	15.3
	SIM	55.9	35.5	63.3*	48.3	14.9	22.6	25.5	28.1	36.8	17.3
	Admix	60.1	45.4	76.2*	56.6	19.8	29.7	34.1	35.9	44.7	18.5
	MaskBlock	53.4	29.3	55.2*	41.9	11.9	18.4	22.6	23.7	32.1	16.2
	US-MM	68.9	49.0	78.8*	63.0	31.3	37.1	39.9	48.6	48.7	20.0
	BSR	68.8	54.1	74.3*	67.2	28.3	40.8	46.3	46.4	53.3	15.8
	CWA	<b>70.8</b>	<b>59.8</b>	<b>80.4*</b>	<b>71.5</b>	<b>34.3</b>	<b>47.0</b>	<b>53.7</b>	<b>52.6</b>	<b>58.8</b>	<b>15.0</b>
DenseNet-121	DIM	68.4	41.2	45.3	97*	20.2	26.8	33.9	35.7	46.1	25.1
	SIM	74.8	45.5	49.6	98.6*	20.9	30.1	38.4	40.6	49.8	25.2
	Admix	81.3	55.9	57.3	<b>99.3*</b>	28	35	43.9	48.1	56.1	23.8
	MaskBlock	67.5	35.3	39.1	95.1*	15	22.7	29.3	31.7	42.0	26.4
	US-MM	82.0	54.4	58.6	98.7*	27.5	35.2	45.8	47.8	56.4	23.8
	BSR	<b>83.8</b>	56.3	61.0	96.6*	29.9	38.6	48.5	48.7	57.9	22.4
	CWA	83.1	<b>60.9</b>	<b>64.7</b>	98.6*	<b>35.1</b>	<b>46.2</b>	<b>52.9</b>	<b>54.8</b>	<b>62.0</b>	<b>20.4</b>

Table 7. Attack success rates (%) of adversarial examples generated using various attack methods across eight classification models under NRP. The surrogate models are cnn-based. \* indicates the surrogate model.

Model	Attack	ResNet-18	ResNet-101	ResNeXt-50	DenseNet-121	ViT	PiT	Visformer	Swin	Mean	Std. Dev.
ViT	DIM	52.5	34.3	34.1	47.9	70.9*	34.4	35.4	39	43.6	13.1
	SIM	57.6	36.1	39.2	52.5	85.3*	38.4	40.5	47	49.6	16.3
	Admix	57.9	37.9	41.4	54.2	<b>86.9*</b>	40.7	41.8	51.3	51.5	16.0
	MaskBlock	56.8	30.3	32.7	47.2	81.6*	30.1	32.6	40.6	44.0	17.9
	US-MM	61.1	40.0	42.8	58.6	84.6*	42.5	44.7	55.0	53.7	15.5
	BSR	66.0	49.9	51.9	62.8	69.1*	55.3	55.1	56.8	58.4	<b>6.9</b>
	CWA	<b>66.7</b>	<b>52.1</b>	<b>53.8</b>	<b>64.1</b>	75.9*	<b>59.1</b>	<b>57.7</b>	<b>58.8</b>	<b>61.0</b>	7.7
PiT	DIM	56	32.2	36.1	48.1	27.2	67.8*	37.2	38.1	42.8	13.5
	SIM	53.1	32	34.5	45.8	24.7	73.5*	35.9	38.1	42.2	15.3
	Admix	54.8	34.7	36	47	25.8	73.8*	39.8	42.8	44.3	14.7
	MaskBlock	56.8	29.7	34.2	44.5	23.1	76.5*	34.8	37.1	42.1	17.2
	US-MM	68.4	37.4	39.2	52.2	29.4	74.4*	43.6	46.0	47.6	14.0
	BSR	68.1	50.2	54.9	65.1	44.1	79.7*	60.0	61.9	60.5	11.1
	CWA	<b>70.6</b>	<b>56.7</b>	<b>59.9</b>	<b>69.3</b>	<b>52.7</b>	<b>85.1*</b>	<b>65.8</b>	<b>67.3</b>	<b>65.9</b>	<b>10.0</b>
Visformer	DIM	59.3	37.8	41.5	53.6	28.6	41.1	76.7*	44.9	47.9	14.9
	SIM	60.7	38.2	40.3	53	27.6	41.2	80.8*	47.8	48.7	16.4
	Admix	61.8	42.5	46.3	59.3	32	47.2	85.6*	54.1	53.6	16.1
	MaskBlock	57.9	32.8	33.8	47.6	20.1	30.8	76.3*	38.5	42.2	17.8
	US-MM	68.8	46.5	52.7	64.1	35.3	50.9	86.4*	58.7	57.9	15.5
	BSR	71.7	52.1	56.8	69.2	40.5	59.3	81.6*	61.4	61.6	12.7
	CWA	<b>73.4</b>	<b>59.0</b>	<b>63.0</b>	<b>73.1</b>	<b>50.8</b>	<b>65.9</b>	<b>87.9*</b>	<b>68.9</b>	<b>67.8</b>	<b>11.1</b>
Swin	DIM	54.6	31.5	33.2	46.1	24.6	33.5	37.4	74.5*	41.9	16.1
	SIM	45.7	25.4	25.9	37.4	14	22	24.5	70.4*	33.2	17.9
	Admix	50.9	25	26.7	40.5	15.2	23.8	27.7	75.2*	35.6	19.4
	MaskBlock	50.1	24.1	24.9	38.3	13.5	20.8	24.9	69.1*	33.2	18.4
	US-MM	52.1	26.1	29.6	43.1	16.2	23.2	28.3	74.3*	36.6	19.0
	BSR	68.8	48.6	51.5	64.6	36.7	54.7	57.0	76.9*	57.4	12.6
	CWA	<b>70.9</b>	<b>54.6</b>	<b>57.7</b>	<b>71.5</b>	<b>45.1</b>	<b>62.4</b>	<b>62.6</b>	<b>83.1*</b>	<b>63.5</b>	<b>11.7</b>

Table 8. Attack success rates (%) of adversarial examples generated using various attack methods across eight classification models under NRP. The surrogate models are transformer-based. \* indicates the surrogate model.



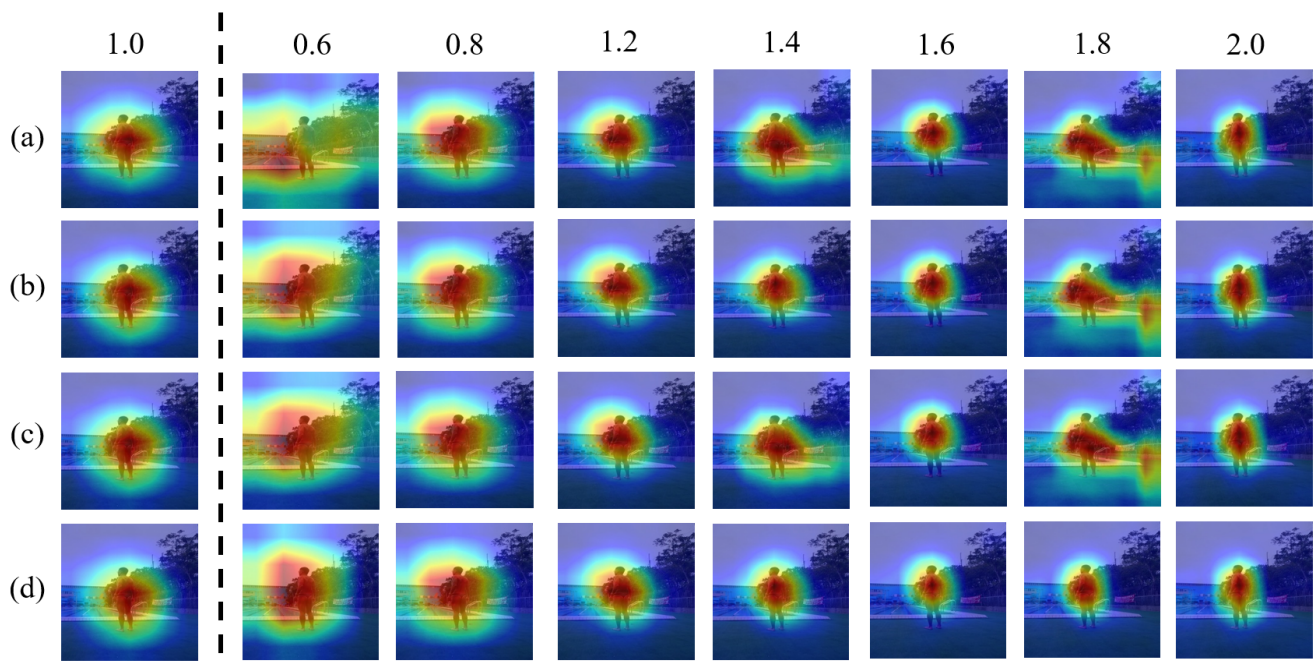


Figure 5. Heatmaps of Different Interpolation Rates Using ResNet-18. (a) Area interpolation; (b) Bicubic interpolation; (c) Bilinear interpolation; (d) Nearest-neighbor interpolation.